Concept and Design of the SMART Spectromicroscope at BESSY II

W. Engel, R. Degenhardt, A.M. Bradshaw, W. Erlebach, K. Ihmann, H. Kuhlenbeck, R. Wichtendahl, H.-J. Freund, R. Schlögl[1], D. Preikszas, H. Rose, R. Spehr, P. Hartel[2], R. Fink, M.R. Weiss, E. Umbach*[3], G. Lilienkamp, Th. Schmidt, E. Bauer[4], G. Benner[5]

[1] Fritz-Haber-Institut der Max-Planck-Gesellschaft, Faradayweg 4-6, D-14195 Berlin, Germany
[2] Technische Hochschule Darmstadt, Angewandte Physik, Hochschulstraße 6, D-64289 Darmstadt, Germany
[3] Universität Würzburg, Experimentelle Physik II, Am Hubland, D-97074 Würzburg, Germany
[4] Technische Universität Clausthal, Leibnizstraße 4, D-38678 Clausthal-Zellerfeld, Germany
[5] LEO Elektronenmikroskopie GmbH, D-73446 Oberkochen, Germany

Abstract. The concept of a new spectromicroscope (SMART = spectromicroscope for all relevant techniques) currently under construction for an undulator beam line at BESSY II is discussed. The design of the optical system is described as well as the modes of operation and the experiments that can be performed. Monochromatic XUV-radiation (tunable within the energy range 20 to 2000 eV) will be provided by a plane-grating monochromator and focussed onto the sample by means of an ellipsoidal mirror. In addition, an electron gun will be installed allowing LEEM, MEM and other forms of microscopy as well as small spot LEED to be performed. With an aberration corrector we expect to achieve a lateral resolution better than 2 nm and to increase considerably the transmission of the optical system compared to previous instruments. An imaging band pass filter corrected to second order will select the energy and the energy band width for the image-forming electrons. The instrument will also allow spectroscopy of photoelectrons from selected small areas of the sample (5 - 500 nm) with an energy resolution of 0.1 eV.

1 Introduction

Photoelectron microscopy with energy selected electrons (termed spectromicroscopy) and spectroscopy of photoelectrons from selected small areas of the sample (termed microspectroscopy) rely on the availability of high brilliance soft X-ray undulators on modern synchrotron radiation sources [1-6]. Some of the

* Project coordinator

so-called third generation sources (ALS in Berkeley, ELETTRA in Trieste) are already in operation; others (BESSY II in Berlin) will be in operation within a short time. Research groups of five German institutions have decided to develop jointly a versatile and high-performance spectromicroscope for an undulator beam line at BESSY II. The aim is to achieve a spatial resolution of about 2 nm and an energy resolution of 0.1 eV for the spectroscopy of photoelectrons. The photon energy will be tunable over a wide range in the XUV giving the possibility of optimising the experimental conditions for particular measurements and also allowing X-ray absorption spectroscopy to be performed. It is intended that image acquisition is so fast that chemical and physical processes at surfaces can be followed with a temporal resolution of about 20 ms.

2 General concept

A high-performance spectromicroscope is necessarily a parallel imaging device and cannot be realised with a scanning-type instrument. In the latter the image is constructed in a serial way, making image formation far too slow for the observation of processes at a sample surface in real time. Further, the lateral resolution of soft X-ray scanning microscopes is determined by the size of the irradiated spot, for which the diffraction limit of the imaging optics will be larger than the desired lateral resolution. In principle, electrons have the capability of forming more highly resolved images than photons of the same energy: the electron mass results in a much shorter wavelength. In order to take advantage of this fact in an electron microscope, however, lens aberrations, in particular the spherical and the axial chromatic aberrations of the objective lens have to be sufficiently small. To compensate for at least the third-order spherical aberration and the second-rank axial chromatic aberration of the objective lens rather sophisticated electron optics is required. The corrected imaging system proposed by Rose and Preikszas [7] will be used in the instrument described here. In addition, an imaging energy band pass filter is needed to select the kinetic energy and the energy bandwidth for the image-forming electrons. This feature will also allow photoelectron spectroscopy to be performed.

The correction of spherical and chromatic aberrations allows the beam aperture and thus the transmission of the objective lens to be considerably enlarged which may be even more important than the improvement of the lateral resolution limit. Although the photon flux density obtainable at BESSY II will be extremely high, lack of intensity will remain a problem in photoemission microscopy, in particular if core electrons are used for imaging. The photoionisation cross sections for core electrons are low and the estimated intensities for typical samples will just allow 2 nm spatial resolution to be achieved [8]. Reaching simultaneously the limits of both the spatial and the energy resolution will, in general, not be possible. The problem of transmission is illustrated in Fig. 1 which shows a section through a quadrant of momentum space. The total photoelectrons emitted from the sample fall in a region of momentum space lying within a sphere the radius of which corresponds to the maximum in the photo-

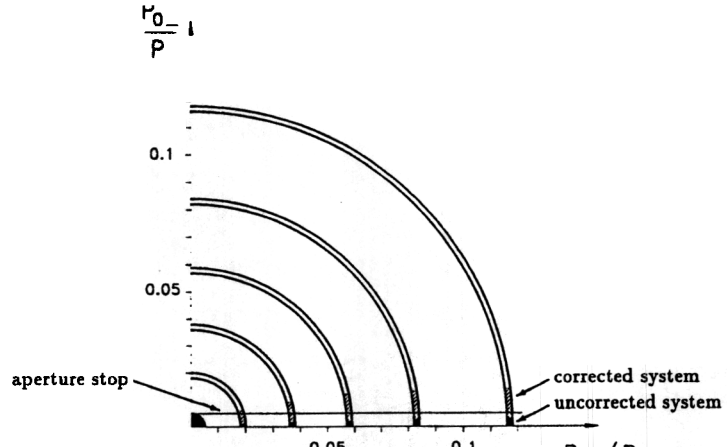

5	20	50	100	200	E_0/eV	E = 15keV
4.8	2.8	1.5	0.81	0.46	T_{corr} %	ΔE = 1eV
1.1	0.7	0.62	0.58	0.56	δ_{corr}/nm	
68.	146.	175.	181.	181.	δ^*_{uncorr}/nm	
0.15	0.07	0.04	0.03	0.02	T_{uncorr} %	
6.0	4.3	3.6	3.2	2.8	δ_{uncorr}/nm	

Fig. 1. Section through a quadrant of momentum space illustrating the small percentage of emitted electrons that can be used for imaging in order to achieve the resolution limits, δ_{corr} and δ_{uncorr}, for the corrected (hatched areas) and uncorrected (black areas) objective lenses, respectively. The corresponding values for the transmission are T_{corr} and T_{uncorr}. δ^*_{uncorr} is the resolution of the uncorrected system calculated for T_{corr}. Data are taken from ref. [9] or derived from data therein. ($p_{0\perp}$, $p_{0\|}$ components of the initial momentum perpendicular and parallel to the optic axis, E_0 initial kinetic energy, p and E momentum and kinetic energy of image-forming electrons, respectively, ΔE energy bandwidth; see text.)

electron kinetic energy. Only a small part of the total volume, however, can be used for imaging, as indicated by the hatched areas in Fig. 1. In order to limit the influence of the remaining chromatic aberration only a small volume between two concentric spheres has to be selected by means of the band pass filter. It determines the mean radius of the spheres (i. e. the initial kinetic energy) and the separation of the spheres (i. e. the width of the energy band for the electrons which pass through the filter and form the image). The remaining spherical aberration requires an aperture stop that limits the volume to the vicinity of the optic axis. The decrease in transmission with increasing kinetic energy, dictated by the condition of optimal lateral resolution, is obvious from the table in Fig. 1. A transmission close to 100% is attained only when photoemission microscopy is carried out in its classical form as a threshold microscopy using photons with

energies slightly higher than the work function. The transmission obtained at the resolution limit for the uncorrected system is extremely small which may be the reason that these calculated resolution limits have never been achieved experimentally. The transmission at the resolution limit for the corrected system, however, is reasonable and represents the more realistic experimental conditions achieved in existing uncorrected instruments. The resolution δ^*_{uncorr} that can be obtained theoretically with the increased transmission of the corrected system, but with the corrector switched off, is also given in Fig. 1. It is interesting to note that these values correspond to the lateral resolution routinely attained in uncorrected systems. The best lateral resolution that has been achieved so far is about 40 nm [1]. Any improvement in lateral resolution by the corrector on the basis of increased transmission would represent important progress even though the theoretical resolution limit may not be achieved. The expected value of 2 nm for the present instrument seems, however, to be realistic because the deterioration in resolution due to misalignments, mechanical instabilities, alternating magnetic fields etc. have already been taken into account.

A schematic overview of the planned spectromicroscope (SMART) is shown in Fig. 2. The beam separator and the tetrode mirror, which simultaneously compensates for the third-order spherical and second-rank axial chromatic aberrations of the objective lens, have been investigated theoretically but so far not been constructed. It is expected that for the construction and experimental tests of these devices more time is needed than that for the rest of the microscope. Thus, in the first stage of the project, the spectromicroscope will not be equipped with these components; an intermediate lens will bridge them. When the beam separator and mirror are incorporated, a field emission electron gun will also be installed opposite the mirror, allowing low energy electron microscopy (LEEM), mirror microscopy (MEM), secondary electron emission microscopy (SEEM), Auger electron emission microscopy (AEEM) [2], and small spot low energy electron diffraction (LEED) to be performed. The imaging band pass filter, an UHV-compatible version of the omega filter developed by Lanio et. al. [10], will be installed in the first stage of the project. The omega filter is fully corrected to second order.

Recently, Rempfer et. al. have reported the simultaneous correction of the spherical and the axial chromatic aberrations of a probe forming objective lens by means of a mirror operated on an optical bench [11]. This represents a first experimental success towards a corrector for the Oregon photoemission microscope [12]. Band pass filters with a lower level of aberration correction are used in the Clausthal instrument [13,14] and in the spectromicroscope called PRISM which has recently been set up for use at the ALS [6].

3 Description of the major components

The SMART spectromicroscope will be installed on an U49 undulator beam line at BESSY II in Berlin. A plane-grating, grazing-incidence monochromator with the designation PM-6 will provide soft X-radiation in the spectral range from

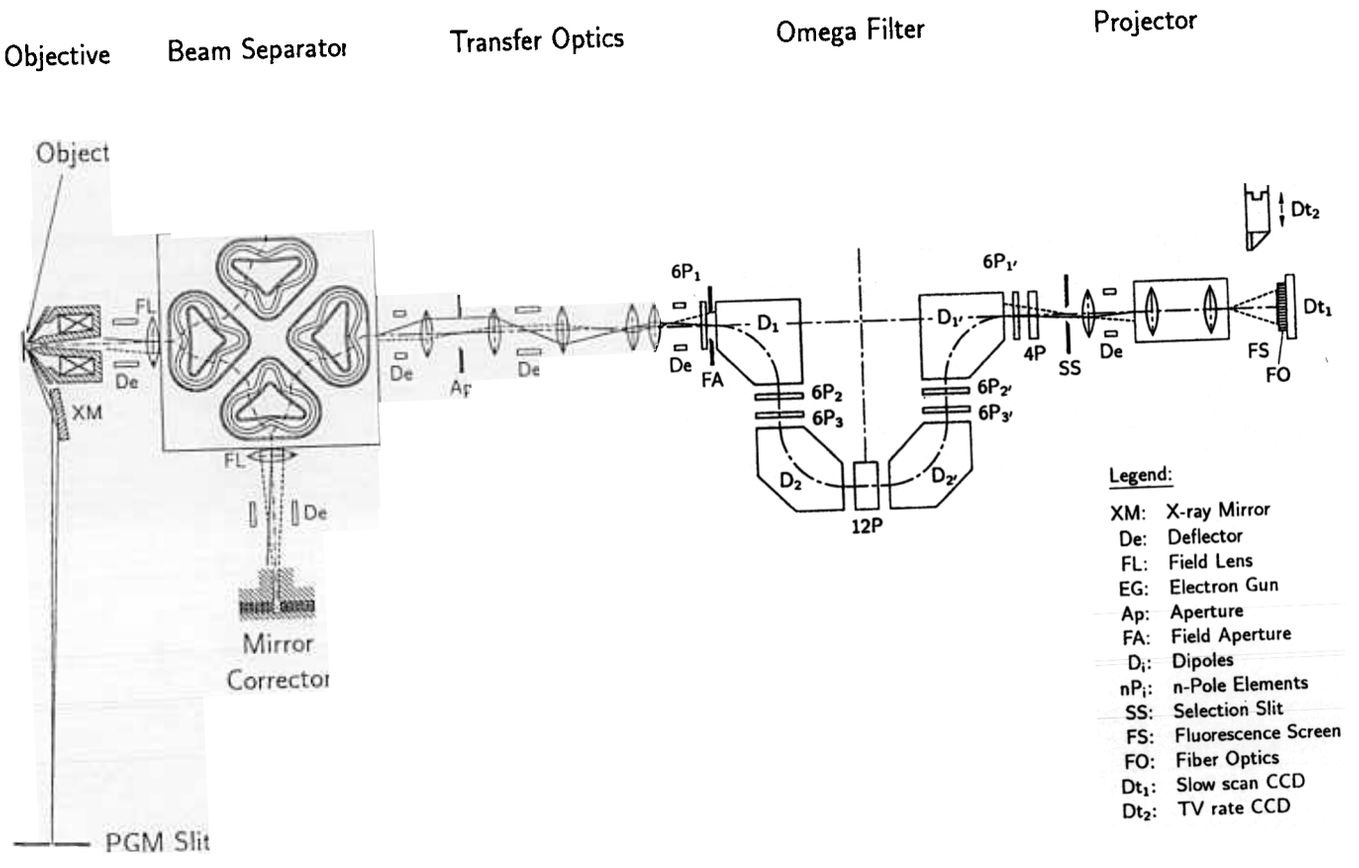
Objective
Beam Separator
Transfer Optics
Omega Filter
Projector
Object
XM
FL
De
FL
De
Mirror
Corrector
PGM Slit
De
Ap
De
6P1
De
FA
D1
6P2
6P3
D2
12P
D2'
6P2'
6P3'
D1'
6P1'
4P
SS
De
FS
FO
Dt1
Dt2
Legend:
XM: X-ray Mirror
De: Deflector
FL: Field Lens
EG: Electron Gun
Ap: Aperture
FA: Field Aperture
Di: Dipoles
nPi: n-Pole Elements
SS: Selection Slit
FS: Fluorescence Screen
FO: Fiber Optics
Dt1: Slow scan CCD
Dt2: TV rate CCD

about 20 eV to 2000 eV. The maximum of its spectral resolving power is about $\nu/\Delta\nu = 10^4$. The exit slit of the monochromator is imaged onto the sample by means of a grazing-incidence ellipsoidal mirror with a demagnification ratio of 10:1, thus irradiating a sample area of $5\mu m \times 10\mu m$. At a photon energy of 400 eV and a bandwidth of 60 meV the flux density at the sample is estimated to be 4×10^9 photons $\mu m^{-2} s^{-1}$. This can be increased by a factor of 10 at the expense of energy resolution by using a second, low-resolution monochromator grating.

The sample is at high negative potential with respect to ground and is the cathode of a so-called cathode lens which is the objective of the microscope. Objective lens, beam separator and tetrode mirror form the corrected imaging system described in ref. [7]. The objective lens is designed as an electrostatic magnetic compound lens. Its magnetic pole piece next to the sample is electrically isolated and can be set at high negative potential. The electric field strength at the sample is then reduced and can even be zero if desired. The acceleration of the emitted photoelectrons then occurs mainly between the two magnetic pole pieces which are at the same time electrodes of a diode. This feature allows rough surfaces to be imaged which would otherwise disturb the electric field in front of the surface and give rise to a severe image deterioration. The cathode lens forms an intermediate image of the sample surface at the entrance of the beam separator where a field lens is located which sets the diffraction plane, i. e. the source image, at infinity. The signs of the third-order spherical and second-rank chromatic aberration coefficients of the proposed electron mirror are opposite to the signs of the corresponding coefficients of the rotationally symmetric magnetic and electrostatic lenses which can thus be compensated [15]. The incident and reflected beams have to be separated by means of magnetic dipole fields which, in general, cause dispersion and second order aberrations. The proposed beam separator, however, does not affect the transferred image by dispersion and second order aberrations, thus representing a remarkable step in the development of mirror-based aberration correction systems. It consists of two quadratic plane pole plates separated by a distance of 7 mm. Four coil triplets are placed into grooves on the inner surface of each pole plate to produce the necessary magnetic fields. The tetrode mirror images with unit magnification and places the corrected image again at the lower edge of the beam separator. The lower right quadrant of the separator then deflects the optic axis back to that of the objective lens and transfers the corrected image to the right hand edge of the separator. The tetrode version of the mirror gives the required flexibility to compensate simultaneously for the spherical and the axial chromatic aberrations of the objective lens in almost all modes of operation.

The transfer optics consists of five electrostatic einzel lenses which form images of the sample and the source (or diffraction pattern) at two fixed planes $z = z_{E2}$ and $z = z_{E1}$, respectively, independent of the selected magnification. This meets the requirements of the omega filter in the imaging mode of the microscope. The plane $z = z_{E1}$ of the source image is in the centre of the last lens and an intermediate sample image is positioned in the centre of the penultimate lens, giving an arrangement that allows focussing of the two images almost independently. Further, the position of the sample image and the source image

(or diffraction pattern) can be exchanged so that the instrument is also capable of producing energy-filtered LEED pattern. Third-order geometric and second-rank chromatic aberrations are negligible for all the planned modes of operation [16]. The first lens of the system places a source image or diffraction pattern at a plane $z = z_{Ap}$ which is fixed for all modes of operation and contains a set of interchangeable diaphragms that are to be used to limit the beam aperture. Such a set is also available in the plane $z = z_{E2}$ at the entrance of the omega filter which will be used to limit the field of view.

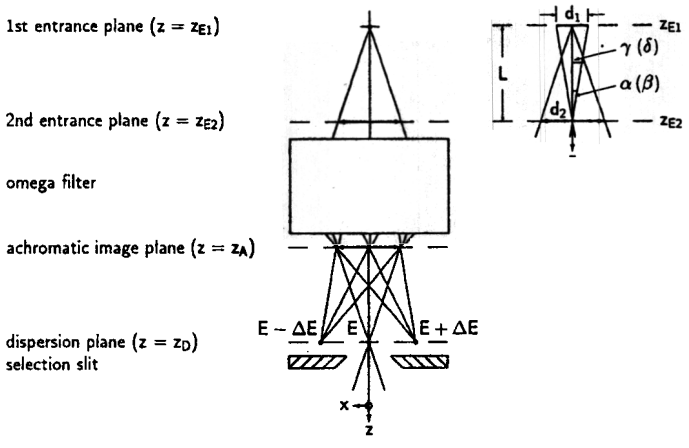

Fig. 3. Conjugate planes (z_{E1}, z_D) and (z_{E2}, z_A) for stigmatic focussing of the omega filter and definition of the ray parameters $\alpha(\beta)$ and $\gamma(\delta)$. d_1 defines the diameter of the source image and d_2 the diameter of the field of view in front of the energy filter. L is the Helmholtz length.

The omega filter consists of four sector magnets each deflecting the optic axis by 90° in such a way that its form resembles the Greek capital letter omega. It images the entrance planes $z = z_{E1}$ and $z = z_{E2}$ stigmatically with unit magnification into the dispersion plane $z = z_D$ and the achromatic image plane $z = z_A$, respectively, as shown schematically in Fig. 3. The spatial dispersion D, which vanishes at the achromatic image plane, has a value of $D = 35$ μm/eV at the dispersion plane for a pass energy of 15 keV. The intermediate sample image (LEED pattern) is formed at $z = z_A$, while the spectrum appears in the plane $z = z_D$. Magnetic energy filters possess 18 linearly independent second-rank aberration coefficients [17]. The aberrations are proportional to $\alpha^k\beta^l\gamma^m\delta^n\kappa^p$ with k+l+m+n+p=2 where $\alpha, \beta, \gamma, \delta$ are the geometrical ray parameters as defined in Fig. 3 and $\kappa = dE/E$ takes into account the energy deviation dE from the pass energy E. With the exception of the axial chromatic aberrations proportional to $\alpha\kappa$ or $\beta\kappa$ in the plane $z = z_A$ and to $\gamma\kappa$ or $\delta\kappa$ in the plane $z = z_D$ as well as the second order dispersions (proportional to κ^2) in both planes, all other second-rank aberration coefficients vanish due to the mid-plane symmetry

or due to appropriate excitation of the sextupole elements [18]. A sextupole field in the mid-plane is generated by a dodecapole which in addition can produce quadrupole fields used to correct for astigmatism due to misalignments. The feasibility of the aberration correction has been demonstrated experimentally by Krahl [19]. The axial chromatic aberrations and the second order dispersion in the achromatic image plane do not affect the resolution limit if the magnification of the intermediate image in front of the omega filter is larger than 310 (even if an energy bandwidth of 5 eV has been chosen). Of particular importance is the correction of second-order aperture aberrations in the dispersion plane, because it guarantees isochromatic filtering in a large field of view. This means in turn that the pass energy does not depend on the position of the image point which is absolutely necessary for unambiguous elemental characterization. The combined effect of the dispersion and the axial chromatic aberration (proportional to $\gamma\kappa$) in the energy selection plane is a tilt of this plane which can result in a blurring of spectra at the detector. This effect can be avoided by readjusting three of the seven sextupole strengths leading to a simultaneous correction of the relevant axial chromatic aberration and the second-order aperture aberration in the energy selection plane. The achievable energy resolution is then determined by the size of the source image and its blurring due to the third-order aperture aberrations in the plane $z = z_D$. An energy resolution of less than 0.1 eV is expected to be obtained for all initial energies E_0.

The projector system consists of 3 electrostatic lenses which project either the sample image (diffraction pattern) at the achromatic image plane or the spectrum at the selection plane onto the image detector. In the first case, the magnification can be varied between 16 and 150. The total magnification of the microscope can then be varied between 500 and 100 000. In the second case, the spectroscopy mode, the magnification can be set between 15 and 60. This is sufficient on the one hand to simultaneously record the transferable spectrum of 35 eV and, on the other hand, to ensure that the energy resolution is not affected by the spatial resolution of the detector. Focussing perpendicular to the dispersive direction can be lifted by means of a quadrupole. A line spectrum is then produced which increases the dynamic range detectable with a CCD detector.

A TEM-1000n slow scan CCD camera and image acquisition system from Tietz Video and Image Processing Systems GmbH (Gauting, Germany) will be used for the recording of high-resolution images and spectra. A second detector system consists of a channel-plate image intensifier combined with a TV-rate CCD camera that can be inserted for alignment purposes and for the observation of relatively fast processes at the sample surface.

4 Modes of operation

The various modes of operation include microscopy, spectroscopy and small spot low energy electron diffraction. In all these cases the pass energy of the omega filter has to be kept constant because a change in the excitation of its sector

magnets requires a readjustment of all multipole correctors and realignment. Setting up the instrument therefore begins with the appropriate excitation of the omega filter which determines the pass energy E (see Fig. 4). The applied acceleration voltage U between sample (cathode) and anode then determines the initial kinetic energy $E_0 = E - eU$ of the electrons at the sample surface which can pass through the omega filter and form the image. E_0 can be varied between 0 and 2000 eV and, in general, will be kept constant during an experiment because a change of E_0 requires refocussing of the objective lens and a readjustment of the mirror corrector. Some exceptions will be discussed below.

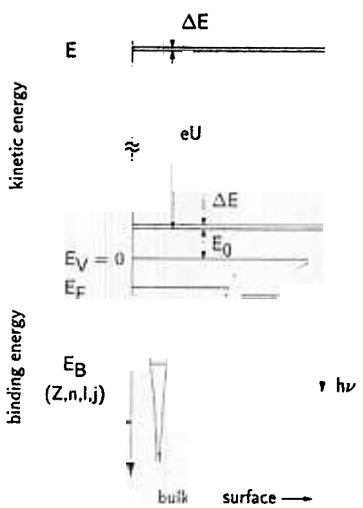

Fig. 4. Schematic energy level diagram for the spectromicroscope (E_P pass energy, ΔE energy window, E_0 initial energy, U acceleration voltage, E_B binding energy, hν photon energy, E_F Fermi level, E_V vacuum level).

4.1 High-resolution microscopy with electrons of selected energy

LEEM, MEM, SEEM, AEEM as well as UV- and X-ray-induced photoemission electron microscopy (PEEM) can be performed with the instrument. (X)PEEM is of main interest because core level photoelectrons can be excited, thus providing a chemical contrast mechanism. There are three different ways of imaging the distribution of a particular element, i.e. of performing elemental mapping. Firstly, core electrons of the element of interest with a binding energy E_B are used. The photon energy hν has to be set within the interval $E_0 + E_B <$ h$\nu <$ $E_0 + E_B + \Delta E$. Optimally, E_0 should be within the energy range 30 – 100 eV for several reasons: (i) E_0 then lies above the large peak of secondary electrons which considerably improves the signal-to-background ratio; (ii) at photon energies near the ionization threshold the cross section for exciting the core electron is close to its maximum; (iii) the experiment is very surface-sensitive because the inelastic mean free path for electrons with kinetic energies in this range is rather small; (iv) the transmission of the objective lens, which decreases with increasing E_0, is still reasonably high. Secondly, Auger electrons characteristic of

the element of interest are imaged by adjusting E_0 to the corresponding kinetic energy E_A of an Auger electron. A considerably higher photon bandwidth can be used in this mode, thus increasing the photon flux density at the sample surface. This method is also very surface-sensitive. Thirdly, secondary electrons can also be used for elemental mapping by taking advantage of the fact that the intensity of secondaries rises steeply when the photon energy exceeds the binding energy of a particular core level. Good contrast is obtained if two images at slightly different photon energies, one above and the other below the binding energy, are taken and the difference is plotted. In order to obtain high intensities, an E_0 value at the intensity maximum of secondaries between 2 and 3 eV is selected. In contrast to the photoelectron and Auger modes, bulk information is also obtained because photoionised atoms in deeper layers contribute substantially to the emission of secondary electrons.

4.2 Spectroscopy in the microscopy mode

In this mode of operation a magnified image of the sample is always produced at the final image detector. The pass energy E of the omega filter and the initial kinetic energy E_0 that is accepted by the optics are fixed, while the photon energy $h\nu$ is tuned in steps through the energy range of interest and an image recorded after each step. Spectra can be recorded simultaneously for all pixels the size of which can be as small as 2×2 nm^2, if sufficient intensity is available. In many cases, however, recording of spectra from some specific areas of interest will be sufficient. Number, position and size of these areas can be selected by the detector system. Various spectroscopies can be performed this way depending on the selected value of E_0.

(i) If E_0 has been chosen far beyond the secondary peak, photoelectron spectroscopy of valence or core levels can be performed in the so-called constant final state (CFS) mode where the final state energy of the detected electrons is fixed. Energy resolution results from a convolution of the transfer functions of both the X-ray monochromator and the omega filter. The latter, however, effectively determines the resolution limit of about 0.1 eV. A spatially resolved chemical analysis with high surface sensitivity can be carried out by choosing optimal settings for E_0 and tuning the photon energy from E_0 to 2000 eV, which causes a brightening in the image at the location of elements when their core electrons fulfill the energy condition for passing through the omega filter. The binding energies of all constituent elements with $E_B < 2000$ eV $- E_0$ can in principle be identified this way.

(ii) X-ray absorption spectroscopy at a surface (XANES, NEXAFS, SEXAFS) is performed by recording the signal of a secondary effect (e.g. secondary electron or Auger emission) induced by the primary core electron excitation as the photon energy is tuned through the energy range of interest. In the case of secondary electrons, E_0 will be set at the intensity maximum of the secondaries. By tuning the photon energy through the available energy range a chemical analysis giving bulk and surface information can also be performed. Micro-XANES measurements with secondary electrons were first performed by Tonner and coworkers

[20]. A significantly improved signal-to-noise ratio and an increase in the surface sensitivity are achieved when E_0 corresponds to an Auger transition in the element of interest. It should be noted that the energy resolution in the X-ray absorption spectroscopy mode is solely determined by the energy resolution of the X-ray monochromator. The energy window of the omega filter is thus a parameter that can be varied in order to optimize the imaging conditions which, in general, will involve a trade-off between contrast, intensity and resolution.
(iii) Photoelectron spectroscopy in the classical sense (ESCA, or XPS, and AES) using photons with fixed energy is also possible in the microscopy mode if E_0 is tuned through the energy range of interest and automatic refocussing of the image is performed. The aberration corrector, however, complicates matters because refocussing necessitates a readjustment of the corrector. This kind of spectroscopy will be practicable only if refocussing and readjustment of the aberration corrector are completely computer-controlled.
(iv) Photoelectron spectroscopy in the CIS (constant initial state) mode is also possible in a computer-controlled instrument by recording images while both E_0 and $h\nu$ are tuned stepwise in such a way that $h\nu - E_0 = E_B$ remains constant.

4.3 Spectroscopy of electrons from selected small sample areas (microspectroscopy)

In this mode the spectrum is projected onto the final image detector which allows parallel recording of spectra within an energy window of 35 eV at an energy resolution of 0.1 eV. Sample areas of interest as small as 5nm in diameter can be selected by the field aperture at the entrance of the omega filter.

4.4 Low energy electron diffraction (LEED)

In order to perform small spot LEED experiments the transfer optics projects the source image rather than the sample image onto the second entrance plane in front of the omega filter. An energy-filtered diffraction pattern which is free of secondary and inelastically scattered electron is thus projected onto the final image detector. Selectable apertures in the electron gun system allow the size of the illuminated sample area to be reduced to 1 μm.

Acknowledgement
The project is supported by the Federal German Ministry of Education, Science, Research and Technology (BMBF) under contract no. 05644WWA9.

References

1. G. Lilienkamp, Th. Schmidt, C. Koziol, and E. Bauer, BESSY Annual Report 1994, p. 469.

2. E. Bauer, T. Franz, C. Koziol, G. Lilienkamp, and T. Schmidt, in *Chemical, Structural and Electronic Analysis of Heterogenous Surfaces on the Nanometer Scale*, edited by R. Rosei (Kluwer Academic Publishing; Dordrecht), in press.
3. J.D. Denlinger, E. Rotenberg, T. Warwick, G. Visser, J. Nordgren, J.-H. Guo, P. Skytt, S.D. Kevan, K.S. McCutcheon, D. Shuh, J. Bucher, N. Edelstein, J.G. Tobin, and B.P. Tonner, Rev. Sci. Instrum. **66**, 1342 (1995).
4. J. Welnak, Z. Dong, H. Solak, J. Wallace, F. Cerrina, M. Bertolo, A. Bianco, S. Di Fronzo, S. Fontana, W. Jark, F. Mazzolini, R. Rosei, A. Savoia, J.H. Underwood, and G. Margaritondo, Rev. Sci. Instrum. **66**, 2273 (1995).
5. E. Umbach, Physica **B 208&209**, 193 (1995).
6. B.P. Tonner, D. Dunham, T. Droubay, J. Kikuma, J. Denlinger, E. Rotenberg, and A. Warwick, J. Electron Spectrosc. Rel. Phen. **75**, 309 (1995).
7. H. Rose and D. Preikszas, Optik **92**, 31 (1992).
8. E. Bauer, Ultramicroscopy **36**, 52 (1991).
9. D. Preikszas, Ph. D. Dissertation D 17, TH Darmstadt (1995).
10. S. Lanio, H. Rose, and D. Krahl, Optik **73**, 56 (1986).
11. G.F. Rempfer, D.M. Desloge, W.P. Skoczylas, and O.H. Griffith, Microscopy and Microanalysis **1** (1997), in press.
12. W.P. Skoczylas, G.F. Rempfer, and O.H. Griffith, Ultramicroscopy **36**, 252 (1991).
13. L.H. Veneklasen, Rev. Sci. Instrum. **63**, 5513 (1992).
14. E. Bauer, Rep. Prog. Phys. **57**, 895 (1994).
15. H. Rose and D. Preikszas, Nucl. Instrum. Methods **A363**, 301 (1995).
16. R. Degenhardt and W. Engel, to be published.
17. H. Rose, Optik **51**, 15 (1978).
18. S. Lanio, Ph. D. Dissertation D 17, TH Darmstadt (1986).
19. H. Rose and D. Krahl, in *Energy-filtering Transmission Electron Microscopy*, edited by L. Reimer (Springer; Berlin, 1995), p. 43.
20. B.P. Tonner and G.R. Harp, J. Vac. Sci. Technol. **A7**, 1 (1989).

This article was processed using the LaTeX macro package with LLNCS style